Structure of the low-lying states in ^{99,101,103,105}Pd

D. Ivanova,[1] S. Lalkovski,[1,*] C. Costache,[2] S. Kisyov,[2,†] C. Mihai,[2] N. Mărginean,[2] P. Petkov,[2] L. Atanasova,[3] D. Bucurescu,[2] R. B. Cakirli,[4] M. P. Carpenter,[5] R. F. Casten,[6] Gh. Căta-Danil,[2] I. Căta-Danil,[2] D. Deleanu,[2] D. Filipescu,[2] N. Florea,[2] I. Gheorghe,[2] D. Ghiţă,[2] T. Glodariu,[2,‡] F. G. Kondev,[5] R. Lica,[2] R. Mărginean,[2] A. Negret,[2] S. Pascu,[2] T. Sava,[2] E. A. Stefanova,[7] L. Stroe,[2] G. Suliman,[2] R. Suvaila,[2] O. Yordanov,[7] and N. V. Zamfir[2]

[1]*Faculty of Physics, Sofia University "St. Kliment Ohridski," Sofia 1164, Bulgaria*
[2]*Horia Hulubei National Institute for Physics and Nuclear Engineering, IFIN-HH, 077125, Bucharest-Magurele, Romania*
[3]*Department of Medical Physics and Biophysics, Medical University - Sofia, 1431 Sofia, Bulgaria*
[4]*Department of Physics, Istanbul University, Istanbul, 34134, Turkey*
[5]*Physics Division, Argonne National Laboratory, Argonne, Illinois 60439, USA*
[6]*Wright Lab, Yale University, New Haven, Connecticut, 06520 USA*
[7]*Institute for Nuclear Research and Nuclear Energy, Bulgarian Academy of Sciences, 72 Tzarigradsko Shaussee, 1784 Sofia, Bulgaria*

(Received 14 June 2021; revised 10 February 2022; accepted 4 March 2022; published 28 March 2022)

The odd-mass $^{99-105}$Pd nuclei were studied via $^{90-96}$Zr(^{12,13}C, xnγ) fusion/evaporation reactions. The beam was provided by the IFIN-HH Tandem accelerator at energies of approximately 50 MeV. Emitted γ rays were detected by the hybrid multidetector system RoSphere. The structure of the low-lying excited states in $^{99-105}$Pd and their gamma-decay pattern are discussed in the framework of the rigid triaxial rotor plus particle model, providing a reasonable description of the low-lying level energies, electromagnetic transition rates, and magnetic moments.

DOI: 10.1103/PhysRevC.105.034337

I. INTRODUCTION

The neutron midshell even-A palladium ($Z = 46$) isotopes present typical textbook examples of transitional nuclei [1] that evolve from harmonic vibrators towards rigid rotors. Historically [2], some of the cadmium ($Z = 48$) nuclei, which are placed two proton holes away from the magic Sn nuclei, have been considered to be the benchmark case of the harmonic vibration model. Recently, driven by a rising amount of new data, an alternate interpretation has been proposed [3,4], and variations on the vibrational perspective have also been suggested [5]. The midshell palladium nuclei are even more deformed than their cadmium isotones but still less deformed than the respective ruthenium ($Z = 44$) and molybdenum ($Z = 42$) neighbors. This interpretation is supported by ground states quadrupole deformation data [6] and γ-ray spectroscopy showing that their yrast level sequences [7] evolve faster than $E \sim J$ typical for the harmonic vibrators, but still slower than $E \sim J(J+1)$ of the axially symmetric rotors. Furthermore, in all neutron midshell even-A palladium nuclei $\Delta J = 1$ bands built on the second 2^+ state are observed. Such sequences are prominent for the transitional nuclei and attributed to deviations from axial symmetry that can be either γ rigid [8] or γ soft [9]. The neutron midshell even-A palladium nuclei are considered to be γ unstable [10], but recent lifetime measurements suggest that rigid triaxial deformation may develop in ^{112,114}Pd$_{66,68}$ nuclei [11,12]. On the extreme-neutron-rich side, the spherical symmetry seems to be restored once again at the semimagic ^{128}Pd$_{82}$ [13] nucleus having an excitation spectrum similar to that of ^{96}Pd$_{50}$ [14]. Indeed, based on theoretical calculations and experimental band structure, some authors suggest [15,16] that oblate deformations may arise in some of the neutron-rich palladium nuclei, which makes the structural changes there even more intriguing to study.

The odd-mass palladium isotopes provide a unique opportunity to further test the nuclear structure of transitional nuclei. Their excitation modes are sensitive not only to the underlying core structure but also to the single-particle orbit that the odd-particle occupies, and to the particle-core interaction. The odd-mass neutron-deficient palladium nuclei have well-established band sequences, but lifetime data are often missing. Being an essential ingredient for the γ-transitions matrix elements calculations, these data provide important information on the structural changes. The present work reports on new half-lives data in the odd-mass palladium nuclei with $A = 99$–105. The new data are analyzed within the rigid triaxial rotor plus particle model (RTRPM) [17] that was

*s.lalkovski@phys.uni-sofia.bg
†Present address: Lawrence Livermore National Laboratory, Livermore, California, USA.
‡Deceased.

TABLE I. Experimental details.

Target	thickness (mg/cm^2)	Backing	thickness (mg/cm^2)	Beam	energy (MeV)	Recoil
^{90}Zr	0.9	Au	1.7	^{12}C	45	^{99}Pd
^{92}Zr	1	Au	2	^{12}C	45	^{101}Pd
^{94}Zr	1	Pb	6.8	^{12}C	45	^{103}Pd
^{96}Zr	1.17	Au	16	^{13}C	55	^{105}Pd

previously used [18,19] for several nuclei of the $A = 100$–120 mass region.

II. EXPERIMENTS AND PROCEDURES

A. Fast-timing experiments

In the present study, half-lives of excited states in medium-mass palladium nuclei $^{99-105}$Pd were measured by using in-beam fast-timing technique [20]. These nuclei were populated in fusion/evaporation reactions with ^{12}C and ^{13}C beams, accelerated by the 9-MV tandem accelerator of IFIN-HH and impinging on $^{90-96}$Zr targets. The typical beam intensity was approximately 20 pnA. The target and beam species, used to populate each of the nuclei considered in the present work, are listed in Table I. γ rays, emitted from the excited nuclear states were detected by the hybrid RoSphere array [20], which comprises eight HPGe and eleven $LaBr_3$:Ce detectors. The system worked in event-by-event mode and the events, where at least three γ rays were detected by two $LaBr_3$:Ce detectors and one HPGe detector in coincidence, were recorded. The sorting procedures applied in the present work are similar to those described in Refs. [20,21].

Even though RoSphere was built in 2009 [20] and the first tests were made in the following years [21,22], the quest for measurements of the shortest half-lives, the in-beam fast-timing method allows, is still ongoing. This led to a continuous improvement of the apparatus and the methods. An essential part of these improvements was the reduction of the time walk effect causing the centroids of the prompt time distributions to appear at positions displaced with respect to the time zero position, introducing systematical errors on measured half-lives. Therefore, time walk is minimized in hardware by careful selection of the constant fraction discriminator (CFD) delay lines and is further reduced by applying off-line corrections during the data analysis [20,23]. Thus, the walk effect can be limited down to a level of 25 ps guaranteed by the CFD manufacturer [24].

To test the time response of the $LaBr_3$:Ce detectors of RoSphere, measurements with ^{60}Co and ^{132}Eu sources were made. They show that RoSphere is a fine-tuned spectrometer having a practically walk-free response at high γ-ray energies, i.e., for $E_\gamma \geqslant 200$ keV [20,21]. In the present work, the RoSphere time response was further analyzed by using in-beam data and by comparison of walk-dependent (centroid shift method) with walk-independent methods (slope method and deconvolution) applied to the same level. In addition, plunger

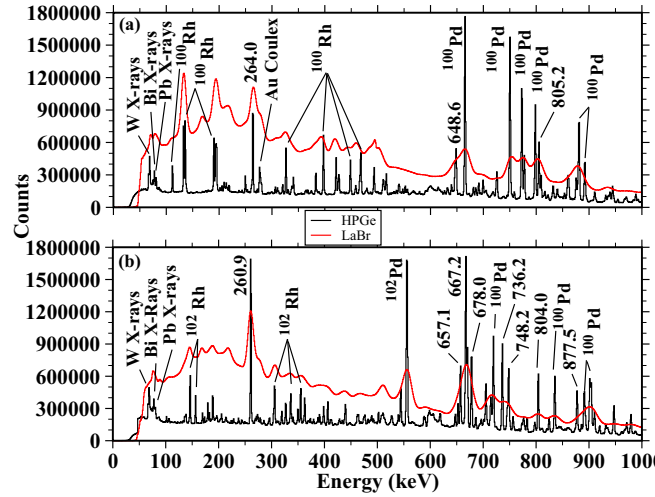

FIG. 1. Total-energy spectra for (a) ^{99}Pd and (b) ^{101}Pd. Gamma-ray energies are in keV. Contamination peaks from the (^{12}C, $2n\gamma$) and (^{12}C, $pn\gamma$) reaction channels, x rays and Au backing Coulomb excitation are also labeled. HPGe spectra are scaled up for visual purpose

measurements were performed, where possible, since they can provide a more stringent test for the shortest half-lives measured at the edge of the fast-timing method applicability.

Sample energy spectra, obtained for ^{99,101}Pd and ^{103,105}Pd in the present study, are shown in Figs. 1 and 2,

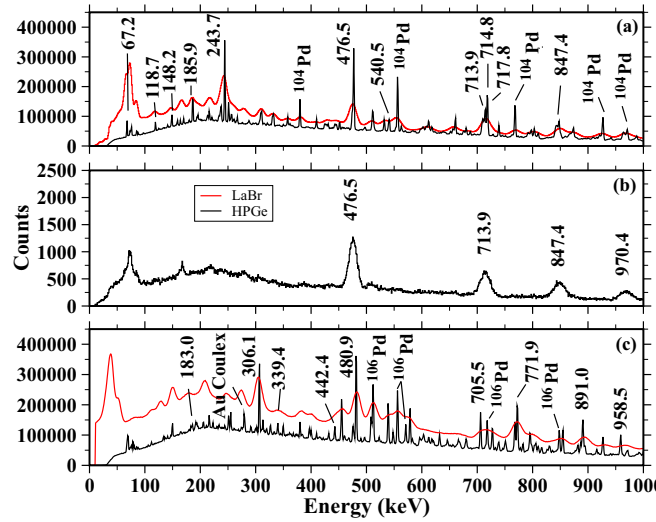

FIG. 2. Energy spectra: (a) summed energy spectra from ^{103}Pd experiment, obtained with the HPGe and $LaBr_3$:Ce detectors of RoSphere. (b) γ rays detected by the $LaBr_3$:Ce detectors in coincidence with the delayed 244-, 451-, and 718-keV γ rays in ^{103}Pd detected in any of the HPGe detectors. (c) γ rays detected by the $LaBr_3$:Ce detectors in coincidence with the 306-keV γ rays in ^{105}Pd detected in any of the HPGe detectors. Gamma-ray energies are in keV. Contamination peaks from the (^{12}C, $2n\gamma$) reaction channels and Au backing Coulomb excitation are also labeled. HPGe spectra are scaled up for visual purposes.

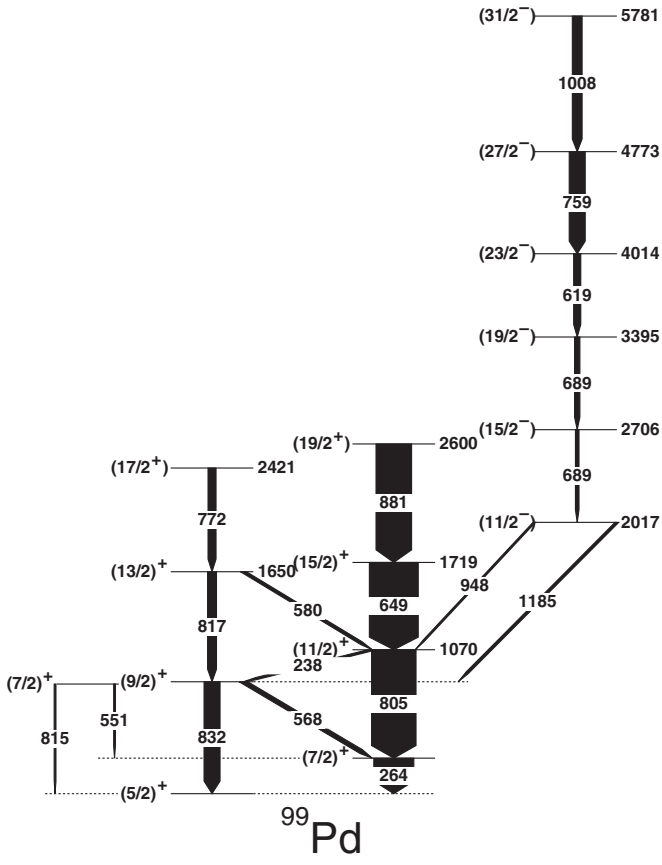

FIG. 3. Partial level scheme of ^{99}Pd. Level energies are rounded off from a least-squares fit to E_γ in keV. J^π values are adopted from Ref. [25].

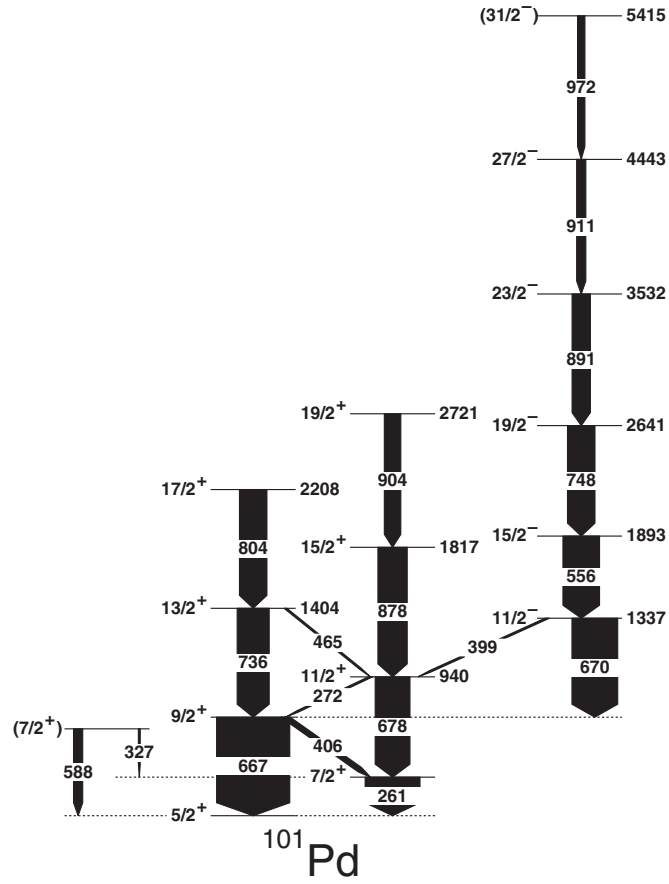

FIG. 4. Partial level scheme of ^{101}Pd. Level energies are rounded off from a least-squares fit to E_γ in keV. J^π values are adopted from Ref. [26].

respectively. Based on $\gamma - \gamma$ coincidence measurements, partial level schemes of $^{99-105}$Pd were constructed and presented in Figs. 3, 4, 5, and 6.

The major part of the new experimental data concerns ^{103}Pd. Figure 2(a) shows a summed energy spectrum taken with the HPGe detectors and is compared with a summed energy spectrum obtained with the $LaBr_3$:Ce scintillators. The energy spectrum shows a dense distribution of γ lines, which is particularly high below 1 MeV. Most of the ^{103}Pd transitions are in this energy range and, due to the worse $LaBr_3$:Ce resolution, often several peaks are superimposed. To obtain a cleaner energy and time spectra with the $LaBr_3$:Ce detectors and to select the decay branch of interest, energy conditions were imposed with the HPGe detectors. Such a gated spectrum is presented in Fig. 2(b) where coincidences with delayed 244-, 451- and 718-keV γ rays detected by the HPGe detectors. The gate, placed on the delayed component of these transitions enhance the peak-to-background ratio and the prompt transitions on top of the $11/2^-$ isomer emerge in Fig. 2(b) more clearly. Similar gated spectra were constructed for all levels considered in the present work.

Furthermore, triple-gated $LaBr_3$:Ce-$LaBr_3$:Ce-HPGe spectra are used to construct the time distributions discussed in Sec. III. This reduces the background considerably and hence helps to reduce the statistical error with which the half-lives were obtained from background-subtracted time spectra.

B. Plunger experiment

Recoil distance Doppler-shift (RDDS) measurements for ^{103}Pd were performed with the Bucharest plunger device [29]. The RoSphere HPGe detectors were arranged in three groups. Five HPGe detectors were placed in a ring at $+37^\circ$ with respect to the beam direction, i.e., at forward angles (FA). Five HPGe detectors were at -37°, i.e., at backward angles (BA) and four detectors at -70°. For the purpose of RDDS measurements, only the rings at $\pm 37^\circ$ were used.

^{103}Pd was produced in (^{12}C, $3n\gamma$) reactions and the beam was accelerated by the IFIN-HH tandem accelerator to $E(^{12}\mathrm{C}) = 56$ MeV. A 1 mg/cm^2 thick ^{94}Zr target was used and the recoils were stopped in a 5 mg/cm^2 Au stopper. In the plunger experiment, the data acquisition was triggered by two HPGe detectors in coincidence. Plunger data were recorded for two weeks of measurements at thirteen target-to-stopper distances from $x = 10$ to 140 μm. For each distance, the data were sorted in two symmetric two-dimensional (2D) (E_γ, E_γ) matrices for forward and backward angles, respectively.

The differential decay curve method (DDCM) [30,31] was used in the data analysis [32] to extract the half-life of the

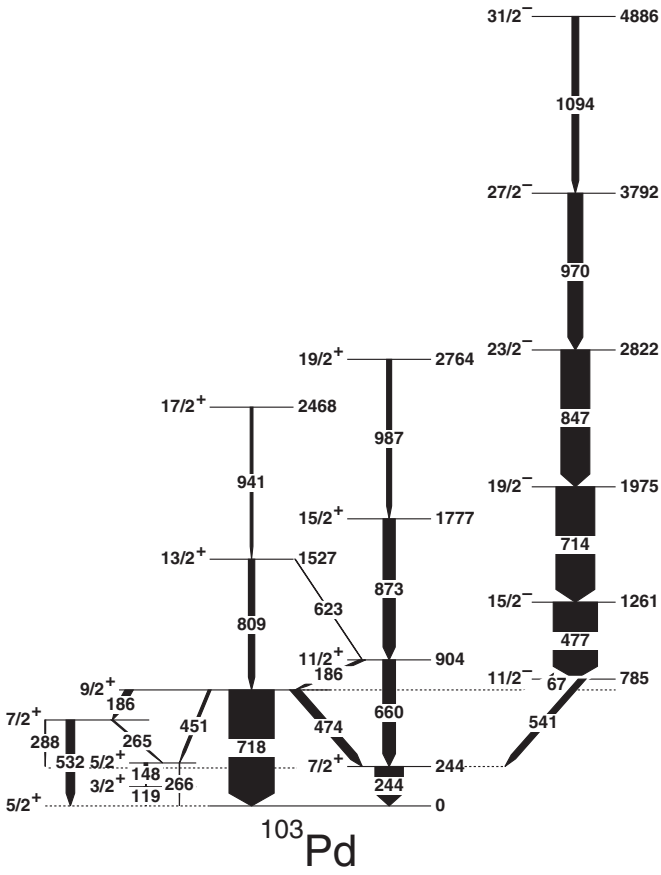

FIG. 5. Partial level scheme of ^{103}Pd. Level energies are rounded off from a least-squares fit to E_γ in keV. J^π values are adopted from Ref. [27].

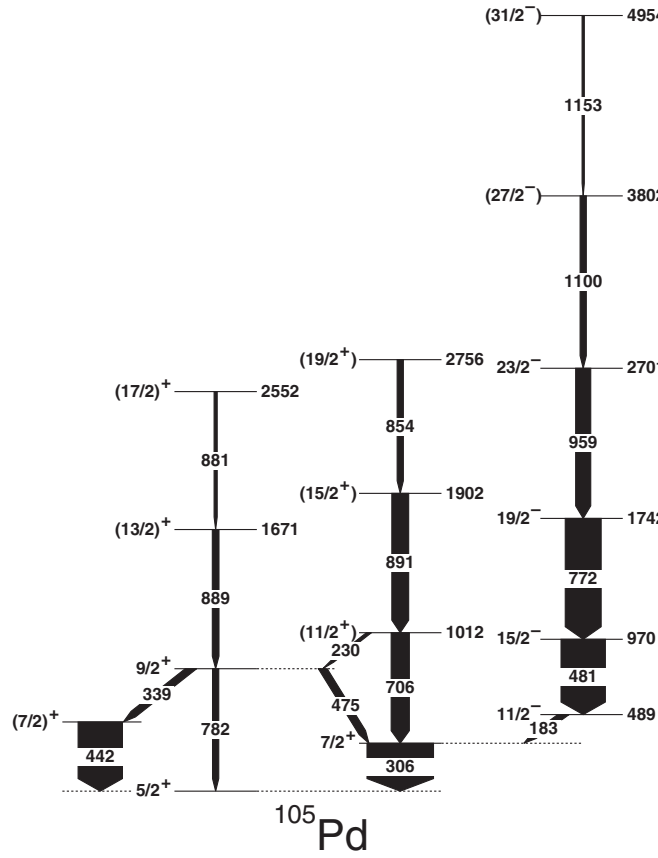

FIG. 6. Partial level scheme of ^{105}Pd. Level energies are rounded off from a least-squares fit to E_γ in keV. J^π values are adopted from Ref. [28].

excited level

$$t_{1/2}(x) = \ln(2)\tau = \ln(2)\frac{\{B_S, A_U\}}{\frac{d\{B_S,A_S\}}{dx}\Big/ v}, \qquad (1)$$

where $\{B_S, A_U\}$ represents the area of the unshifted decaying transition A_U obtained from an energy spectrum gated on the shifted feeding transition B_S. $\{B_S, A_S\}$ represents the area of the shifted decaying transition A_S, obtained from the same energy spectrum gated on the shifted feeding transition B_S and v is the mean recoil velocity. The mean velocity of the recoils $\beta = 0.87(5)\%$ was obtained as a weighted average, calculated from the centroids of the shifted and unshifted components of the 477-, 714-, 847- and 660-keV transitions observed at different plunger settings. Sample energy spectra around the 477- and 714- keV transitions are shown in Fig. 7 (left) as a function of the plunger-to-stopper distance.

III. EXPERIMENTAL RESULTS

A. ^{99}Pd

The half-life of $(7/2_1)^+$ state in ^{99}Pd was measured in the present study for the first time. Figure 8(a) presents the time spectrum for this state obtained from the coincidence between the 264- and 805-keV transitions detected by the $LaBr_3$:Ce

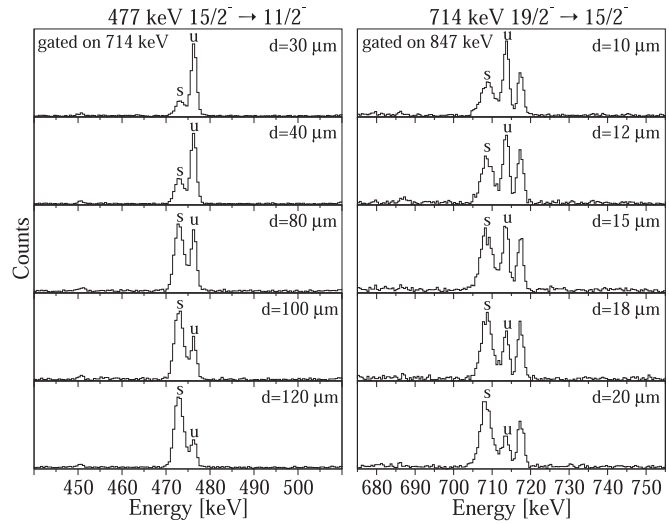

FIG. 7. ^{103}Pd energy spectra around the 477- and 714-keV peaks. Shifted and unshifted components are denoted with "s" and "u," respectively. The 718-keV contaminating line is the $7/2^+ \rightarrow 5/2^+$ transition. This transition is in coincidence with the highly converted 67-keV isomeric transition depopulating the 25-ns isomer at 785 keV.

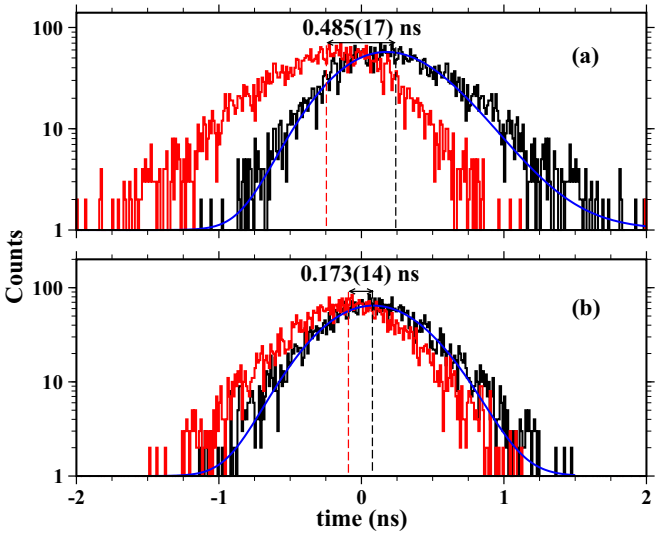

FIG. 8. Time spectra for the $7/2_1^+$ state in (a) ^{99}Pd and (b) ^{101}Pd, respectively. Here and in the following two figures, the centroid shift difference equals twice the lifetime τ of the level.

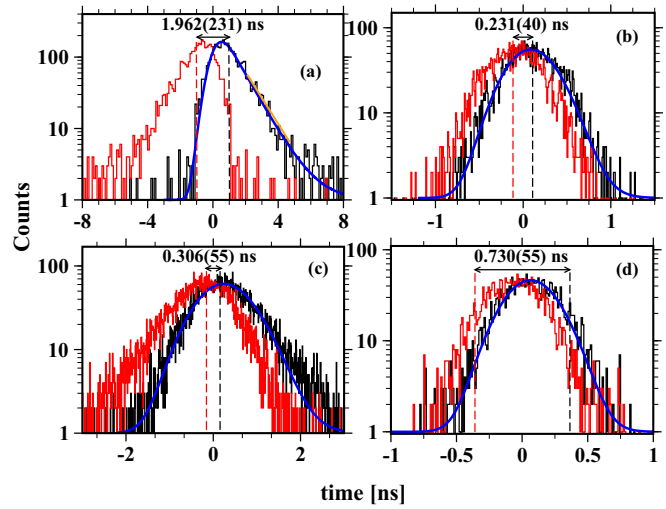

FIG. 9. Time spectra for the (a) $3/2_1^+$, (b) $7/2_1^+$, (c) $9/2_1^+$, and (d) $15/2_1^-$ states in ^{103}Pd.

detectors. The time spectrum was cleaned with a gate on 649-keV transition detected with the HPGe detectors. A half-life of 168(6) ps was obtained from the centroid shift method, applied for the two symmetric time distributions, and 157(4) ps was obtained from deconvolution method [33,34]. The two values are consistent with each other and their weighted average $T_{1/2} = 160(5)$ ps has been adopted in Table II.

The $(7/2_1)^+$ level decays to the $(5/2_1)^+$ ground state via the 264-keV $\Delta J = 1$ transition. Typically, such transitions are of $M1 + E2$ nature, but no experimental mixing ratio data are available for 264γ [25]. Indeed, similar states and decays are observed in the heavier ^{101,103,105}Pd with negligible $7/2^+ \rightarrow 5/2^+ M1 + E2$ mixing ratios measured only in ^{103,105}Pd. Therefore, for the purpose of the present work, we tentatively assume the 264-keV transition is $M1$. Thus, the electromagnetic transition rate is $B(M1; 264\gamma) = 7.28 \times 10^{-3}(24)$ W.u. Here, and in the text below, the electron conversion coefficients $\alpha_{\rm calc}$ are calculated with BrIcc [36].

B. ^{101}Pd

The time spectrum shown in Fig. 8(b) was obtained from the coincidences between the 261- and 678-keV transitions detected by the $LaBr_3$:Ce detectors, and the 878-keV transition detected by the HPGe detectors. A half-life of 60(5) ps was obtained from the centroid shift method and 64(3) ps from the deconvolution. It has to be noted, however, that our half-life is considerably shorter than the half-life $T_{1/2} = 0.7(2)$ ns reported in Ref. [37], where the generalized centroid-shift method was applied for coincidences between one Pilot B plastic scintillator and one HPGe detector. The reason for this discrepancy may be that, in Ref. [37], the half-life was measured by the deviation of the 261-keV point from the time-zero curve. The time-zero curve in Ref. [37] was obtained from the transitions in ^{100}Pd and the side feeding effect seems to have been undermined, leading to a half-life much longer than the one measured in the present work.

The $7/2_1^+$ level decays to the $5/2_1^+$ ground state via 261-keV transition of $M1$ nature [26] with $B(M1; 261\gamma) = 2.06 \times 10^{-2}$ (17) W.u. The arguments to adopt here the multipolarity adopted by NNDC are the same as for the analogous transition in ^{99}Pd. A second branch from this state populates the $3/2_1^+$ state at 80 keV via a stretched $E2$ transition with $B(E2; 180\gamma) = 9(4)$ W.u. This weak branch is not observed in the present experiment. The $B(E2)$ value here is obtained with 179.7 keV γ rays and the branching ratio taken from Ref. [26].

C. ^{103}Pd

1. $3/2_1^+$ *state*

Prior to the present study, the half-life of the $3/2_1^+$ state in ^{103}Pd was measured from radiochemically separated ^{103}Ag source [38]. $T_{1/2} = 1.9(4)$ ns was deduced from the Compton electrons generated by the 119- and 148-keV γ rays detected in coincidence by two 1 in. × 1 in. plastic scintillators. The time spectrum was deconvoluted and the parameters of the prompt component were estimated with a ^{22}Na source, emitting two γ rays of 511 keV, which may lead to incorrect evaluation of the prompt response distribution (*PRD*) position. Indeed, a different half-life $T_{1/2} = 0.70(3)$ ns was deduced from ISOL mass-separated activity [39] and $119\gamma(t)$ analysis. However, experimental details were not given by the authors. $T_{1/2} = 0.63(6)$ ns was also measured in Ref. [40].

In the present study, the $3/2_1^+$ half-life was measured by using the RoSphere fast-timing setup. It is listed in Table II along with subnanosecond half-lives of other states in ^{103}Pd. Two symmetric time spectra, obtained from the coincidences between the 119- and 148-keV transitions detected with the $LaBr_3$:Ce scintillators are presented on Fig. 9(a). To reduce the background, the spectra are also gated with the HPGe detectors on transitions from the band based on the $11/2_1^-$ isomer. The half-life of the $3/2_1^+$ state was used to check the walk

TABLE II. Experimental data for $^{99-105}$Pd: level energy (E_{level}) and spin and parity (J^{π}) assignments for the initial level; number of counts in the time spectrum N; half-life obtained from the centroid shift method $T_{1/2}^{centr}$; $T_{1/2}^{dec}$ is deduced from deconvolution; full width at half maximum of the prompt distribution (FWHM) obtained via deconvolution; $T_{1/2}^{pl}$ is the half-life obtained from RDDS measurements and $T_{1/2}^{adopt}$ is the most reliable value adopted for the half-life of the level; γ-ray energies of the deexciting transitions E_γ and their branching ratios I_γ; γ-ray multipolarities λM and mixing ratios δ; electron conversion coefficients $\alpha_{\rm calc}$ calculated with BrIcc [36].

Nucleus E_{level} (keV)	J^{π} ($\hbar$)	$N/10^3$	$T_{1/2}^{centr}$ (ps)	$T_{1/2}^{dec}$ (ps)	FWHM (ps)	PRD (ps)	$T_{1/2}^{pl}$ (ps)	$T_{1/2}^{adopt}$ (ps)	E_γ (keV)	I_γ[a]	λM[a]	δ[a]	α_{calc}
^{99}Pd													
[25]													
264	$7/2_1^+$	5.9	168(6)	157(4)	740(12)	3(4)		160(5)	264.0(7)	100	$M1$		0.0275(5)
^{101}Pd													
[26]													
261	$(7/2_1)^+$	5.9	60(5)	64(3)[b]	767(10)[b]	0.6(5)		60(5)	260.9(7)	100	$M1$		0.0283(5)
									179.7(6)	0.5	$E2$		0.173(4)
^{103}Pd													
[27]													
119	$3/2_1^+$	3.6	680(80)	743(16)	1200(90)	70(50)		743(16)	118.7(5)	100	$M1+E2$	0.090 (15)	0.239(5)
244	$7/2_1^+$	4.2	80(14)[b]	68(3)[b]	603(10)[b]	13(5)		80(14)	243.7(6)	100	$M1+E2$	−0.085 (15)	0.0340(6)
									124.4(6)	2	$E2$		0.640(15)
267	$5/2_2^+$	1.1	106(19)	91(28)[c]	580(125)[c]	3.1(21)		106(19)	266.3(10)	52	$M1+E2$	−0.14 (6)	0.0272(6)
									148.2(7)	100	$M1$		0.1275(25)
718	$9/2_1^+$	11.2	253(19)	229(8)	1223(24)	16(7)		212(7)	717.8(10)	100	$E2$		0.00223(4)
		3.9	203(14)	198(9)	1264(27)	5(12)			473.9(9)	13	$M1+E2$		0.0067(4)
		2.6	189(21)	163(13)	1259(37)	5.2(17)			451.0(6)	7	$E2$		0.00811(12)
		11.5	225(15)	216(5)	1505(15)	12(8)			186.0(6)	15	$M1+E2$	−0.12 (6)	0.0702(19)
1262	$15/2_1^-$	2.6	41(4)[b]	46(3)[b]	453(9)[b]	10(5)	17.9(3)	17.9(3)	476.5(9)	100	$E2$		0.00688(11)
1976	$19/2_1^-$						2.70(21)	2.70(21)	713.9(11)	100	$E2$		0.00226(3)
^{105}Pd													
[28]													
306	$7/2_1^+$	3.2	92(8)	118(4)	460(12)	15(5)		92(8)	306.1(6)	100	$M1+E2$	0.055 (3)	0.0188(3)
970	$15/2_1^-$	4.8	14(9)	36(2)	458(6)	13(3)		28(4)	480.9(8)	100	$E2$		0.00670(10)

[a]From Ref. [35].
[b]Weak transition, insufficient statistics to deduce $T_{1/2}$.
[c]High Compton background.

correction, performed in the present study. The position of the prompt distribution [$PRD = 0.07(5)$ ns] was determined from a deconvolution of the time spectrum into Gaussian and exponent, where $T_{1/2}^{w.a.} = 0.69(3)$ ns was held fixed to the half-life of the state obtained as a weighted average of the literature values 0.70(3) ns and 0.63(6) ns [39,40]. Also, a fit to the slope of the time distribution performed for $T \geqslant 1.5$ ns gives $T_{1/2}^{slope} = 0.69(6)$ ns, which provides a PRD independent method for estimation of $T_{1/2}$ and is consistent with $T_{1/2}^{w.a.}$ and $T_{1/2}^{centr} = 0.68(8)$ ns as well as with the literature values 0.70(3) ns and 0.63(6) ns from Refs. [39,40].

The level decays to the $5/2_1^+$ ground state via a transition of mixed $M1+E2$ multipolarity with $\delta = 0.090(15)$ [27]. The reduced transition rates are $B(M1; 119\gamma) = 1.42 \times 10^{-2}(5)$ W.u. and $B(E2; 119\gamma) = 7.3(25)$ W.u.

2. $7/2_1^+$ state

The half-life of the $7/2_1^+$ state in ^{103}Pd was measured for the first time in the present study. The state decays via two transitions with energies of 244 and 125 keV, respectively. The time spectrum shown in Fig. 9(b) is constructed by using the coincidences between 541- and 244-keV γ rays. The 125-keV decay branch is weak and is not observed in the present experiment. Cleaning conditions were imposed with the HPGe detectors.

The half-life of the state was deduced from the centroid shift method $T_{1/2}^{centr} = 80(14)$ ps, shown in Fig. 9(b), and from deconvolution $T_{1/2}^{dec} = 68(3)$ ps of the time spectrum. These values are in agreement with the upper limit $T_{1/2} < 0.2$ ns deduced in Ref. [37] and are listed in Table II.

The level decays via two transitions—a stretched 125-keV $E2$ transition with $B(E2; 7/2^+ \rightarrow 3/2^+) = 160(40)$ W.u. and a 244-keV $M1+E2$ transition with $\delta = -0.085(15)$ [27] and $B(M1; 7/2^+ \rightarrow 5/2^+) = 1.8 \times 10^{-2}(4)$ W.u. and $B(E2; 7/2^+ \rightarrow 5/2^+) = 1.9(8)$ W.u.

3. $5/2_2^+$ state

The half-life of the $5/2_2^+$ state $T_{1/2} = 106(19)$ ps was measured for the first time in the present work. It was determined

by using the centroid-shift method and validated by deconvolution data analysis.

The level decays via two transitions. A pure 148-keV $M1$ transition ($\delta = 0.005$ [27]) with $B(M1; 5/2_2^+ \rightarrow 3/2^+) = 3.8 \times 10^{-2}(7)$ W.u. and a mixed $M1 + E2$ 266-keV transition with $\delta = -0.14(6)$ [27] and $B(M1; 5/2_2^+ \rightarrow 5/2_1^+) = 3.4 \times 10^{-3}(7)$ W.u. and $B(E2; 5/2_2^+ \rightarrow 5/2_1^+) = 0.8(+9, -6)$ W.u., respectively.

4. $9/2_1^+$ state

The half-life of the $9/2_1^+$ state in ^{103}Pd is also obtained for the first time in the present study. The level decays via four transitions of different energies. A set of half-lives was obtained from the time spectra gated on the feeding 67-keV transition and each of the deexciting transitions. To obtain the half-life of the level, centroid shift and convolution methods were applied to each of the four spectra. The results from the half-life analysis are listed in Table II. In general, the half-lives obtained from the centroid shift method and deconvolution are consistent, but for each spectrum the deconvolution method systematically underestimates it. The time spectra, presented on Fig. 9(c), are obtained from the coincidences between the 474- and 67-keV transitions registered by the $LaBr_3$:Ce detectors. To reduce the background contribution additional conditions with the HPGe detectors were imposed on the prompt transitions placed on top of the $11/2^-$ isomer.

The state decays [27] via a branch of transitions—two pure $E2$ transitions with energies of 718 and 451 keV and two transitions of mixed multipolarities, i.e., 474 and 186 keV. The 186-keV transition mixing ratio is $\delta = -0.12\,(6)$ [27]. There is no experimental data for the 474-keV transition mixing ratio. A mixing ratio $\delta = 1$ was assumed by the authors. Therefore the obtained reduced transition strengths $B(E2; 9/2_1^+ \rightarrow 5/2_1^+) = 0.358(14)$ W.u., $B(M1; 9/2_1^+ \rightarrow 7/2_1^+) = 3.2 \times 10^{-5}$ W.u., $B(E2; 9/2_1^+ \rightarrow 7/2_1^+) = 0.25(3)$ W.u., $B(E2; 9/2_1^+ \rightarrow 5/2_2^+) = 0.26(4)$ W.u., $B(M1; 9/2_1^+ \rightarrow 7/2_2^+) = 1.75 \times 10^{-3}(25)$ W.u. and $B(E2; 9/2_1^+ \rightarrow 7/2_2^+) = 0.7(+8, -5)$ W.u., respectively, are only tentative.

5. $15/2_1^-$ state

The half-life of the $15/2_1^-$ state in ^{103}Pd was obtained by using the in-beam fast-timing method [20] and compared with RDDS measurements with the Bucharest plunger device [41]. The RDDS data for the $15/2_1^-$ state are shown in Fig. 10 (left). They show the intensity of the shifted (s) and unshifted (u) components of the 477-keV peak as functions of the plunger-to-stopper distance. The data analysis shows that the half-life of the state is $T_{1/2} = 17.9(3)$ ps, which is in reasonable agreement with $T_{1/2} = 21.6(30)$ ps measured previously in Ref. [42] by using the recoil distance Doppler-shift method.

Also, the $15/2_1^-$ half-life was directly measured by using the fast-timing method. The time spectra, shown in Fig. 9(d), were obtained by gating on the 477- and 714-keV transitions with the $LaBr_3$:Ce detectors. A gate below the $11/2_1^-$ isomer was imposed on any of the HPGe detectors to clean the energy and the time spectra. The centroid position is found to

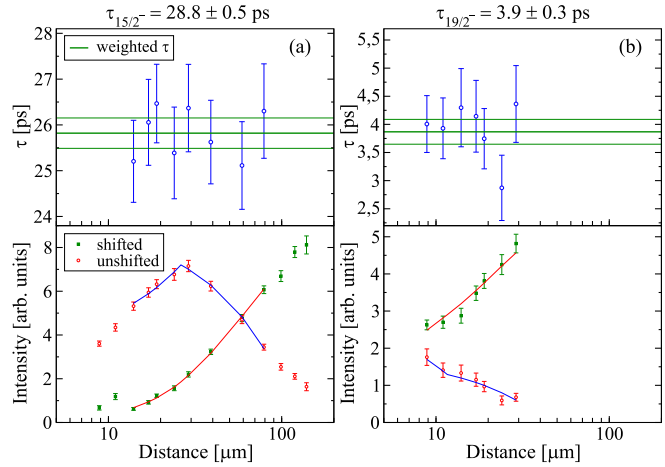

FIG. 10. RDDS data for $15/2^-$ (left) and $19/2^-$ (right) states in ^{103}Pd. Data were analyzed with the NAPATAU program [32].

be at 41(4) ps with respect to the arbitrary offset. A 46(3) ps were obtained from the deconvolution of the time spectrum. Given that the half-life of the level is at the limit of the applicability of the method, fine *PRD* corrections were made by using the in-beam data for ^{102}Pd produced in the same experiment. There, the first 2^+ state in the even-even nucleus is populated by a 719-keV transition and decays via a 556-keV transition, which resembles the $15/2_1^-$ case in ^{103}Pd. The *PRD* was estimated to 15.5 (14) ps, given that the apparent half-life $T_{1/2}^{ap} = PRD + T_{1/2} = 27(6)$ ps, determined from centroid-shift measurements for the 2^+ level in ^{102}Pd, is a superposition of the *PRD* and the half-life of the level $T_{1/2} = 11.5$ (8) ps [35]. Thus, the half-life of the $15/2^-$, corrected for the *PRD*, is 26(4) ps, which is in a good agreement with the RDDS measurements performed in the present study and in Ref. [42].

The level decays via a single γ transition with energy of 477 keV and $B(E2) = 44.6(9)$ W.u.

6. $19/2_1^-$ state

$T_{1/2} = 2.70(21)$ ps was obtained for the first time in the present RDDS experiment. The half-life of the level was obtained by using the intensities of the shifted and unshifted 714-keV peaks shown in Fig. 10 (right). To facilitate the analysis only the HPGe detectors at backward angles were used, given that at forward angles the shifted component of the 714-keV transition overlaps with the 718-keV transition from the $9/2_1^+$ level. The electromagnetic transition rate is $B(E2; 19/2^- \rightarrow 15/2^-) = 39(3)$ W.u.

D. ^{105}Pd

1. $7/2_1^+$ state

Prior to our study, the level half-life was estimated [28] to be 71(8) ps from the Coulex data. In the present study, the half-life of this state was determined from the delayed coincidences between the 306- and 706-keV transitions shown in Fig. 11(a). The time spectrum was additionally cleaned with a gate on HPGe detectors imposed on 891-, 854- or

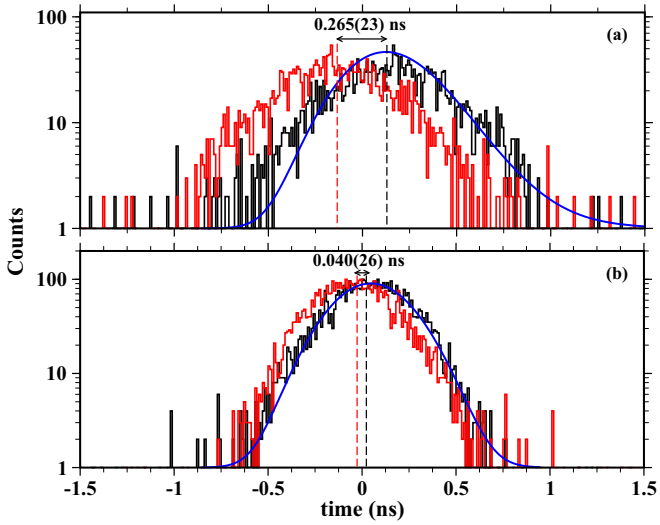

FIG. 11. Time spectra for the (a) $7/2_1^+$ and (b) $15/2_1^-$ states in ^{105}Pd.

539-keV prompt transitions. The half-life, obtained from the centroid shift method is 92(8) ps and 118(4) ps is obtained from deconvolution.

The level decays via a single γ transition of mixed multipolarity and $\delta = 0.055$ (2). Hence, the $B(M1; 7/2^+ \rightarrow 5/2^+) = 8.2 \times 10^{-3}(8)$ W.u. and $B(E2; 7/2^+ \rightarrow 5/2^+) = 0.23(3)$ W.u., respectively

2. $15/2_1^-$ state

The half-life of the $15/2_1^-$ state in ^{105}Pd was measured for the first time in the present work. The time spectrum, shown in Fig. 11(b), is obtained from the delayed coincidences between the 481- and 772-keV γ rays. The time spectrum is additionally cleaned with gates on 959-, 1100- and 1153-keV prompt transitions, imposed on the RoSphere HPGe detectors. The half-life, measured in the present experiment, is $T_{1/2} = 28(4)$ ps. The level decays via a pure $E2$ transition with $B(E2; 481\gamma) = 27(4)$ W.u. Similarly to the ^{103}Pd case, the decay properties of the $7/2_1^+$ and $15/2_1^-$ states are listed in Table II.

IV. DISCUSSION

The positive-parity bands observed in $^{99-105}$Pd are not unique for these palladium isotopes. Similar band-like sequences were observed in the heavier isotopes, as shown in Fig. 12. After the abrupt decrease in energy, from $^{97}Pd_{51}$ to $^{99}Pd_{53}$, the yrast level energies remain nearly constant with the neutron number. This behavior seems to be weakly correlated with the 2^+ level energies of the even-even palladium cores decreasing with neutron number towards neutron midshell. In contrast with the yrast states, the $3/2^+$ level shows a different trend. It oscillates around the $7/2^+$ state, and, in ^{101}Pd, it is closer to the $5/2^+$ ground state than in any of the other isotopes in Fig. 12. Indeed, a similar trend is observed in the ruthenium isotopic chain [43], where the $3/2+$ state becomes the ground state in ^{103,105}Ru. Figure 12 presents also the

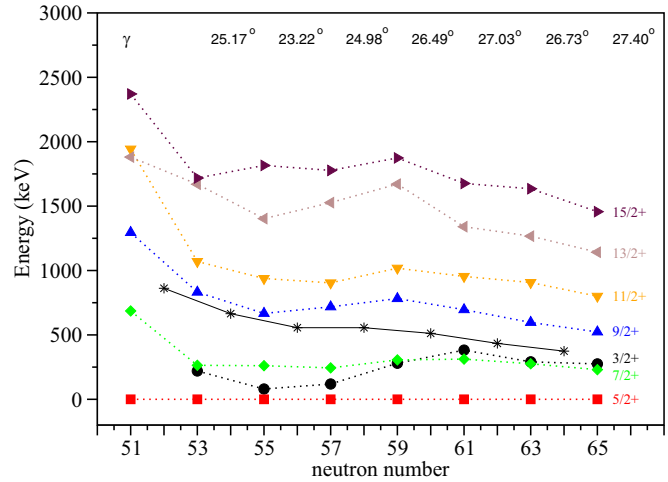

FIG. 12. Low-lying positive-parity yrast states in some odd-mass palladium isotopes compared with the core 2^+ level energies denoted with * symbols. Even-even palladium nuclei are considered to be the cores of the odd-A palladium isotopes. Triaxial parameter γ is determined from the neighboring even-even nuclei considered to be the core.

evolution of the triaxial parameter γ calculated as

$$\gamma = \frac{1}{3}\arcsin\sqrt{\frac{9}{8}[1-(X-1)^2/(X+1)^2]}, \qquad (2)$$

where X denotes the level energy ratio $E_{2_2^+}/E_{2_1^+}$, obtained from the core's 2^+ states [8]. This systematics shows that small changes in γ seem to have large impact on the $3/2^+$ level energies. Indeed, the linear correlation coefficient between the $3/2^+$ level energy and the triaxial parameter γ is $\mathrm{corr}(\gamma, E_{3/2^+}) = 0.86$, calculated as

$$\mathrm{corr}(\gamma, E_{3/2^+}) = \frac{\sum_i(\gamma_i-\overline{\gamma})\sum_i(E_{i,3/2}-\overline{E_{3/2}})}{\sqrt{\sum_i(\gamma_i-\overline{\gamma})^2\sum_i(E_{i,3/2}-\overline{E_{3/2}})^2}}, \qquad (3)$$

where $\overline{\gamma}$ and $\overline{E}_{3/2}$ are γ and $E_{3/2}$ mean values estimated from the sample shown in Fig. 12. Apparently, this effect is less pronounced in the yrast band sequence. However, fine effects can be detected by using the staggering calculated as

$$Stg_I = E_I - \frac{(I+1)E_{I-1} + IE_{I+1}}{2I+1}. \qquad (4)$$

Stg_I introduced in Ref. [44] describes the placement of the level E_I with respect to the neighboring levels E_{I-1} and E_{I+1}. Results for $^{99-105}$Pd nuclei are presented in Fig. 13(a). All isotopes have identical staggering patterns, except for the $^{101}Pd_{55}$ isotope, the same nucleus that has a $3/2^+$ level unusually low in energy.

To further test the triaxiality in these nuclei rigid-triaxial-rotor-plus-particle model [17] calculations were performed. The model Hamiltonian [17] is $H = \sum_{k=1}^{3}(I_k^2 - 2I_k j_k +$

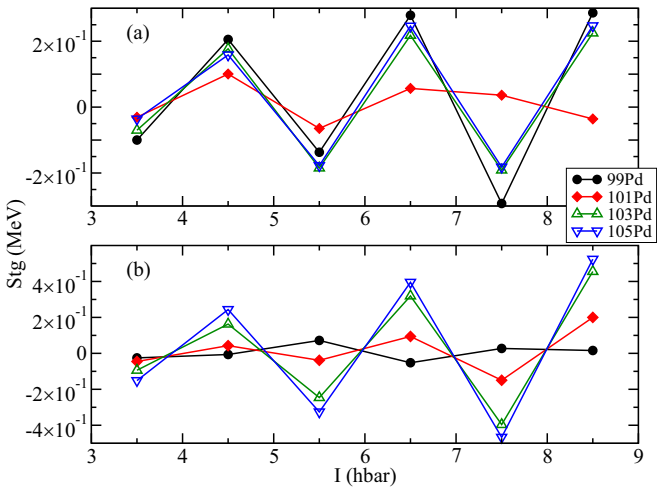

FIG. 13. Staggering function obtained from the (a) experimental data and (b) theoretical calculations for $^{99-105}$Pd.

$j_k^2)/2\Im_k + H_{part}$, where $\vec{I} = \vec{R} + \vec{j}$ is the total angular momentum with $\vec{R}$ and $\vec{j}$ being the core and the single-particle angular momenta, respectively. $\Im_k = \frac{4}{3}\Im_0 \sin^2(\gamma + k\frac{2}{3}\pi)$ is the triaxial rotor moment of inertia. H_{part} is the single-particle Hamiltonian. The single-particle wave functions were calculated with the GAMPN code, which is part of the ASYRMO package [45]. The Nilsson parameters $\kappa_4 = 0.070$, $\mu_4 = 0.39$ and $\kappa_5 = 0.062$ and $\mu_5 = 0.43$ [46] were used for the fourth and fifth oscillators shells, respectively. The initial values of the deformation parameters ϵ_2 and ϵ_4 were deduced from the neighboring even-even palladium nuclei by using Grodzin's equation and from the finite-range droplet model calculations performed in Ref. [15]. The core moment of inertia is calculated from the E_{2^+} excitation energy, deduced also from the neighboring even-even nuclei. The parameter of triaxiality γ is calculated from the $E_{2_2^+}/E_{2_1^+}$ energy ratios and Eq. (2). The particle-rotor level energies were then calculated in a strong-coupling basis by using the ASYRMO code [45]. A Coriolis attenuation parameter $\chi = 0.8$ [45] was used. To obtain a better fit to the experimental level energies, the deformation, moment of inertia, and triaxiality parameters were varied. The set of parameters, for which the best description was found, are listed in Table III. This procedure was applied earlier in Refs. [19] and [18], for example.

In the case of ^{103}Pd, the positive-parity states were calculated for $\gamma = 0^\circ$ to 60° with a step of 5°. On the prolate side the level energies are almost independent of γ, which is consistent with the present observations. A similar approach has been applied for the rest of the palladium nuclei considered here. Sample theoretical level schemes are shown in Fig. 14 for the odd-A $^{99-105}$Pd nuclei, and compared with the experimental data. The overall description of the experimental level energies is good at the low- and medium- spin regimes. At higher spins, the theoretical level energies overestimate experimental energies. This is due to the back-bending effect observed in the odd-mass palladium positive-parity bands [47], which is not accounted for by the model. The overall description of the staggering effect is also good, as shown in Fig. 13.

TABLE III. RTRPM parameters for the positive-parity bands in $^{101-105}$Pd.

Nucleus	^{99}Pd$_{53}$	^{101}Pd$_{55}$	^{103}Pd$_{57}$	^{105}Pd$_{59}$
ϵ_2	+0.10	+0.15	+0.17	+0.19
ϵ_4	−0.07	−0.07	−0.04	−0.04
γ	32.0°	32.0°	32.0°	26.48°
χ	0.8	0.8	0.8	0.8
E2PLUR (MeV)	0.48	0.52	0.54	0.54

Table IV presents a summary of the reduced transition probabilities calculated for several transitions deexciting the low-lying positive-parity yrast states in $^{99-105}$Pd. The $7/2_1^+$ state feeds the $5/2_1^+$ ground state via a hindered $M1$ transitions. The hindrance factor is two-three units and is overall well reproduced by the RTRPM calculations.

Similar hindrance factors were observed earlier in some of the odd-mass cadmium nuclei [48] and were attributed [37] to l-forbidden $M1$ transitions that link single-particle states with $\Delta l = 2$, suggesting that the two states involved in this transition are of rather pure single-particle nature. This interpretation is also supported by the small $E2$ components. Also, a strong argument supporting the single-particle nature of these states is the large spectroscopic factors, measured for the $5/2_1^+$ and $7/2_1^+$ states in ^{101,103,105}Pd from neutron transfer reactions [35]. In addition, the magnetic moments measured for the ground states in ^{101}Pd and ^{105}Pd are $(-)0.66(2)\mu_N$ and $-0.642(3)\mu_N$ [49], respectively. Therefore, the leading component of the ground-state wave function is assumed to be $\nu d_{5/2}$. If the γ-decay mechanism is the same as in the Cd nuclei, then the main component of the $7/2^+$ state is $\nu g_{7/2}$.

The magnetic moments of the $5/2^+$ ground states, calculated for ^{101,105}Pd within the RTRPM, are $-0.927\mu_N$ and $-0.86\mu_N$, respectively, and are also in a reasonable agreement with the experimental values.

The $3/2_1^+$ states decay to the ground state via transitions of mixed $M1 + E2$ multipolarity. The $M1$ components are hindered with respect to the Weisskopf units by two to three orders of magnitude, which is similar to the $B(E2; 7/2_1 \rightarrow 5/2^+)$ transition rates. The RTRPM calculations describe well the transition hindrance.

The experimental $B(E2; 3/2_1 \rightarrow 5/2^+)$ in ^{101}Pd is large, but the uncertainty is also big. For the rest of the palladium nuclei, the experimental transition strengths are several Weisskopf units. The $B(E2)$ values for those mixed-multipolarity transitions are not correctly reproduced, which might be related to discrepant mixing ratio coefficients.

The experimental magnetic moment of the $3/2^+$ state in ^{105}Pd is $-0.074(13)\mu_N$ [49]. This value is far from the Schmidt values—$\mu(\nu d_{3/2}) = 1.148\mu_N$ and $\mu(\nu d_{5/2}) = -1.913\mu_N$, but its sign suggests a dominant $\nu d_{5/2}$ component of the wave function, since $\nu d_{3/2}$ is much higher in energy. This is also in agreement with the spectroscopic factor for this state, observed from (p, d) reactions, which is relatively larger when compared with the spectroscopic factors for the

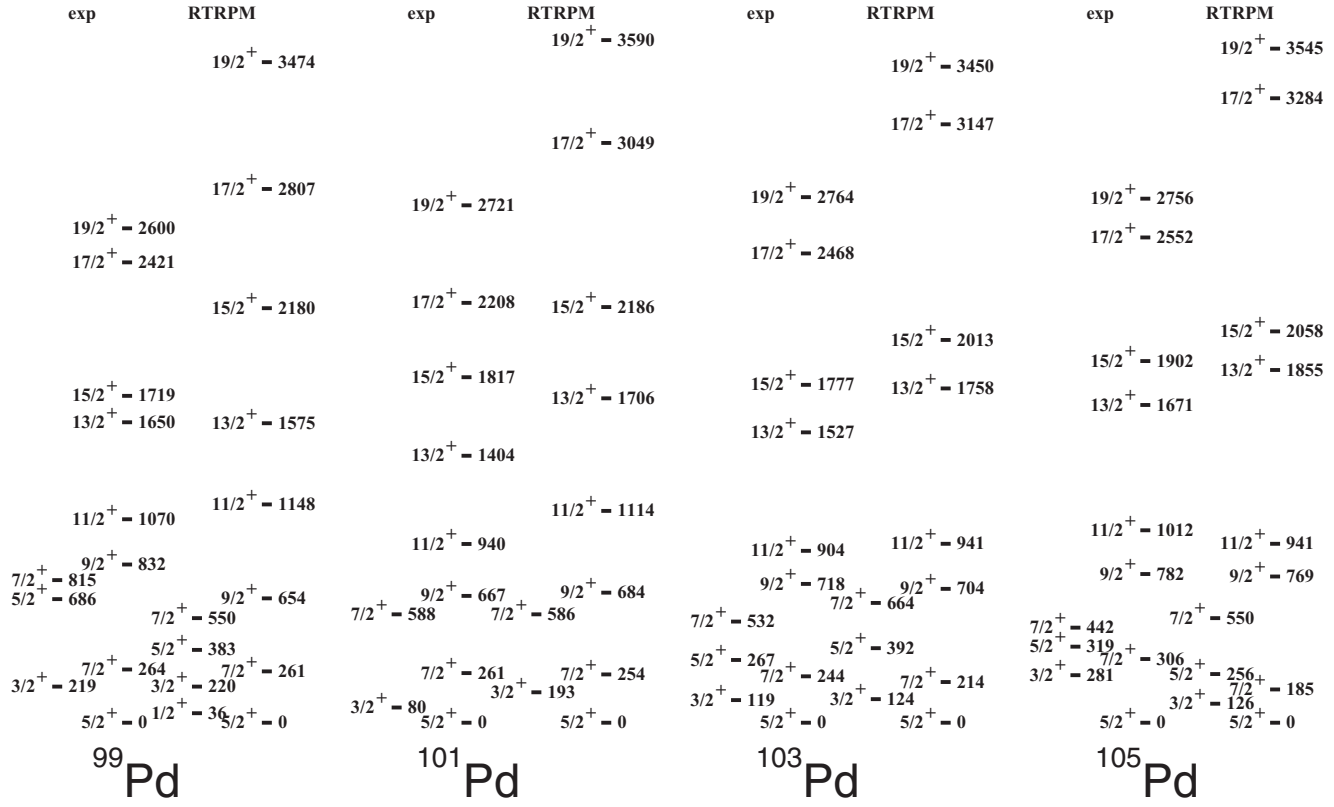

FIG. 14. Experimental and theoretical partial schemes of the yrast and some near-yrast levels in the odd-mass $^{99-105}$Pd nuclei. Model parameters are given in Table III.

respective states in the neighboring palladium nuclei. Therefore, we tentatively interpret this as a $\nu d_{5/2} \times 2^+$ state.

V. CONCLUSION

Low-lying states in $^{99-105}$Pd were excited in four fusion-evaporation reactions. Lifetime measurements of their low-lying excited states were performed by using fast-timing technique realized with the hybrid RoSphere detector array. In addition, lifetimes of negative-parity states in ^{103}Pd were measured by using the recoil distance Doppler-shift method. The new data are analyzed within the rigid triaxial rotor plus particle model. A good description of the low-lying states energies and transition rates in these palladium isotopes is achieved. This result is interesting since the even-even Pd isotopes have been interpreted in the past as γ-soft nuclei. Given that RTRP model satisfactorily describes the $^{99-105}$Pd data, we can assume that the odd particle polarizes the γ-unstable palladiums' cores towards rigid triaxiality. However, the alternative interpretation, where RTRP model describes well unstable nuclei when γ is similar to the average triaxial deformation of the soft core, cannot be ruled out completely. Nevertheless, both scenarios require significant deviations from axial symmetry to explain the structure of the $^{99-105}$Pd odd-mass nuclei.

TABLE IV. Summary of experimental and theoretical reduced transition probabilities for transitions deexciting low-lying positive-parity yrast states in $^{99-105}$Pd. $B(M1)$ and $B(E2)$ are given in W.u. Gamma-ray energies E_γ are from the present experiment; branching ratios are from the ENSDF file [35]; conversion coefficients are from BrIcc [36]; lifetime data are from present experiment except for the 3/2+ states in ^{101,105}Pd where they are adopted from ENSDF.

$B(\lambda L; J_i^\pi \to J_f^\pi)$		^{99}Pd	^{101}Pd	^{103}Pd	^{105}Pd
$B(M1;\ 7/2_1^+ \to 5/2_1^+)$	Expt.	7.28×10^{-3} (24)	2.00×10^{-2}(17)	1.8×10^{-2} (4)	8.2×10^{-3} (8)
$B(M1;\ 7/2_1^+ \to 5/2_1^+)$	RTRPM	2.28×10^{-3}	1.14×10^{-3}	1.73×10^{-3}	3.27×10^{-3}
$B(E2;\ 7/2_1^+ \to 5/2_1^+)$	Expt.			1.9 (8)	0.23 (3)
$B(E2;\ 7/2_1^+ \to 5/2_1^+)$	RTRPM	0.47	0.01	0.08	0.12
$B(M1;\ 3/2_1^+ \to 5/2_1^+)$	Expt.		3.7×10^{-3} (6)	1.42×10^{-2} (5)	2.03×10^{-2} (22)
$B(M1;\ 3/2_1^+ \to 5/2_1^+)$	RTRPM	7.28×10^{-2}	2.02×10^{-3}	1.2×10^{-2}	1.65×10^{-2}
$B(E2;\ 3/2_1^+ \to 5/2_1^+)$	Expt.		90 (50)	7.3 (25)	4.6 (7)
$B(E2;\ 3/2_1^+ \to 5/2_1^+)$	RTRPM	2.69	22	33	36

ACKNOWLEDGMENTS

This work is supported by the Bulgarian National Science Fund contract number KP-06-N48/1. Work at ANL was supported by the U.S. Department of Energy, Office of Nuclear Physics under Contract No. DE-AC02-06CH11357. D.I., S.L., and S.K. are thankful to Professor Dr. N. Minkov for the constructive discussions.

[1] R. F. Casten, *Nuclear Structure from a Simple Perspective* (Oxford University Press, New York, 2000).

[2] A. Bohr and B. R. Mottelson, *Nuclear Structure* (World Scientific, Singapore, 1998), Vol. 1.

[3] P. E. Garrett, EPJ Web Conf. **66**, 02039 (2014).

[4] P. E. Garrett, T. R. Rodriguez, A. D. Varela, K. L. Green, J. Bangay, A. Finlay, R. A. E. Austin, G. C. Ball, D. S. Bandyopadhyay, V. Bildstein, S. Colosimo, D. S. Cross, G. A. Demand, P. Finlay, A. B. Garnsworthy, G. F. Grinyer, G. Hackman, B. Jigmeddorj, J. Jolie, W. D. Kulp, K. G. Leach, A. C. Morton, J. N. Orce, C. J. Pearson, A. A. Phillips, A. J. Radich, E. T. Rand, M. A. Schumaker, C. E. Svensson, C. Sumithrarachchi, S. Triambak, N. Warr, J. Wong, J. L. Wood, and S. W. Yates, Phys. Rev. Lett. **123**, 142502 (2019).

[5] A. Leviatan *et al.*, EPJ Web Conf. **178**, 05003 (2018); Phys. Rev. C **98**, 031302(R) (2018).

[6] N. J. Stone, At. Data Nucl. Data Tables **111-112**, 1 (2016).

[7] S. Lalkovski and N. Minkov, J. Phys. G **31**, 427 (2005).

[8] A. S. Davidov and G. F. Filippov, Nucl. Phys. **8**, 237 (1958).

[9] L. Wilets and M. Jean, Phys. Rev. **102**, 788 (1956).

[10] S. Lalkovski *et al.*, Eur. Phys. J. A **18**, 589 (2003).

[11] E. R. Gamba, A. M. Bruce, S. Lalkovski, M. Rudigier, S. Bottoni, M. P. Carpenter, S. Zhu, J. T. Anderson, A. D. Ayangeakaa, T. A. Berry, I. Burrows, M. C. Gallardo, R. J. Carroll, P. Copp, D. M. Cullen, T. Daniel, G. F. Martinez, J. P. Greene, L. A. Gurgi, D. J. Hartley, R. Ilieva, S. Ilieva, F. G. Kondev, T. Kroll, G. J. Lane, T. Lauritsen, I. Lazarus, G. Lotay, C. R. Nita, Z. Podolyak, V. Pucknell, M. Reed, P. H. Regan, J. Rohrer, J. Sethi, D. Seweryniak, C. M. Shand, J. Simpson, M. Smolen, E. A. Stefanova, V. Vedia, and O. Yordanov, Phys. Rev. C **100**, 044309 (2019).

[12] A. Esmaylzadeh, V. Karayonchev, G. Hafner, J. Jolie, M. Beckers, A. Blazhev, A. Dewald, C. Fransen, A. Goldkuhle, L. Knafla, and C. Muller-Gatermann, Phys. Rev. C **103**, 054324 (2021).

[13] H. Watanabe *et al.*, Phys. Rev. Lett. **111**, 152501 (2013).

[14] H. Mach, A. Korgul, M. Gorska, H. Grawe, I. Matea, M. Stanoiu, L. M. Fraile, Y. E. Penionzkevich, F. D. Santos, D. Verney, S. Lukyanov, B. Cederwall, A. Covello, Z. Dlouhy, B. Fogelberg, G. DeFrance, A. Gargano, G. Georgiev, R. Grzywacz, A. F. Lisetskiy, J. Mrazek, F. Nowacki, W. A. Plociennik, Z. Podolyak, S. Ray, E. Ruchowska, M. G. Saint-Laurent, M. Sawicka, C. Stodel, and O. Tarasov, Phys. Rev. C **95**, 014313 (2017).

[15] P. Moeller, A. J. Sierk, T. Ishikawa, and H. Sagawa, At. Data Nucl. Data Tables **109-110**, 1 (2016).

[16] Y. X. Luo *et al.*, Nucl. Phys. A **919**, 67 (2013).

[17] S. E. Larsson, G. Leander, and I. Ragnarsoon, Nucl. Phys. A **307**, 189 (1978).

[18] S. Lalkovski, A. M. Bruce, A. M. DenisBacelar, M. Gorska, S. Pietri, Z. Podolyak, P. Bednarczyk, L. Caceres, E. Casarejos, I. J. Cullen, P. Doornenbal, G. F. Farrelly, A. B. Garnsworthy, H. Geissel, W. Gelletly, J. Gerl, J. Grebosz, C. Hinke, G. Ilie, D. Ivanova, G. Jaworski, S. Kisyov, I. Kojouharov, N. Kurz, N. Minkov, S. Myalski, M. Palacz, P. Petkov, W. Prokopowicz, P. H. Regan, H. Schaffner, S. Steer, S. Tashenov, P. M. Walker, and H. J. Wollersheim, Phys. Rev. C **88**, 024302 (2013).

[19] S. Lalkovski, D. Ivanova, E. A. Stefanova, A. Korichi, P. Petkov, J. Kownacki, T. Kutsarova, A. Minkova, D. Bazzacco, M. Bergstrom, A. Gorgen, B. Herskind, H. Hubel, A. Jansen, S. Kisyov, T. L. Khoo, F. G. Kondev, A. Lopez-Martens, Z. Podolyak, G. Schonwasser, and O. Yordanov, Phys. Rev. C **89**, 064312 (2014).

[20] N. Mărginean, *et al.*, Eur. Phys. J. A **46**, 329 (2010).

[21] S. Kisyov, S. Lalkovski, N. Mărginean, D. Bucurescu, L. Atanasova, D. L. Balabanski, G. Căta-Danil, I. Căta-Danil, J. M. Daugas, D. Deleanu, P. Detistov, D. Filipescu, G. Georgiev, D. Ghita, T. Glodariu, J. Jolie, D. S. Judson, R. Lozeva, R. Mărginean, C. Mihai, A. Negret, S. Pascu, D. Radulov, J. M. Regis, M. Rudigier, T. Sava, L. Stroe, G. Suliman, N. V. Zamfir, K. O. Zell, and M. Zhekova, Phys. Rev. C **84**, 014324 (2011).

[22] S. Kisyov *et al.*, J. Phys. Conference Series **366**, 012027 (2012).

[23] J.-M. Régis, G. Pascovici, J. Jolie, and M. Rudigier, Nucl. Instrum. Methods Phys. Res., Sect. A **622**, 83 (2010).

[24] Model 935 Quad Constant-Fraction 200-MHz Discriminator Operating and Service Manual.

[25] E. Browne and J. K. Tuli, Nucl. Data Sheets **145**, 25 (2017).

[26] J. Blashot, $A = 101$ mass chain evaluation, www.nndc.bnl.gov/ensdf

[27] D. De Frenne, Nucl. Data Sheets **110**, 2081 (2009).

[28] S. Lalkovski, I. Timar, and Z. Elekes, Nucl. Data Sheets **161-162**, 1 (2019).

[29] C. Mihai, Ph.D. thesis, IFIN-HH Romania, 2012.

[30] A. Dewald, S. Harissopulos, and P. von Brentano, Z. Phys. A **334**, 163 (1989).

[31] G. Böhm, A. Dewald, P. Petkov, and P. von Brentano, Nucl. Instrum. Methods Phys. Res., Sect. A **329**, 248 (1993).

[32] T. Pissulla and B. Saha, Napatau 2.0 or Tk-Lifetime-Analysis, July 2013.

[33] L. Boström, B. Olsen, W. Schneider, and E. Matthias, Nucl. Instrum. Methods **44**, 61 (1966).

[34] B. Olsen and L. Boström, Nucl. Instrum. Methods **44**, 65 (1966).

[35] ENSDF data file, www.nndc.bnl.gov/ensdf

[36] T. Kibédi, T. W. Burrows, M. B. Trzhaskovskaya, P. M. Davidson, and C. W. Nestor Jr., Nucl. Instrum. Methods Phys. Res., Sect. A **589**, 202 (2008).

[37] W. Andrejtscheff,L. K. Kostov, L. G. Kostova, P. Petkov, M. Senba, N. Tsoupas, Z. Z. Ding, and C. Tuniz, Nucl. Phys. A **445**, 515 (1985).

[38] H. Bakhru, R. I. Morse, and I. L. Preiss, Can. J. Phys. **47**, 419 (1969).

[39] P. G. Hansen *et al.*, Phys. Lett. B **28**, 415 (1969).

[40] R. B. Begzhanov *et al.*, Dokl. Akad. Nauk. Uzb. SSR **1**, 24 (1972).

[41] C. Mihai, A. A. Pasternak, D. Filipescu, M. Ivaşcu, D. Bucurescu, G. Căta-Danil, I. Căta-Danil, D. Deleanu, D. Ghita,

T. Glodariu, Y. N. Lobach, N. Mărginean, R. Mărginean, A. Negret, S. Pascu, T. Sava, L. Stroe, G. Suliman, and N. V. Zamfir, Phys. Rev. C **81**, 034314 (2010).

[42] S. F. Ashley, P. H. Regan, K. Andgren, E. A. McCutchan, N. V. Zamfir, L. Amon, R. B. Cakirli, R. F. Casten, R. M. Clark, W. Gelletly, G. Gurdal, K. L. Keyes, D. A. Meyer, M. N. Erduran, A. Papenberg, N. Pietralla, C. Plettner, G. Rainovski, R. V. Ribas, N. J. Thomas, J. Vinson, D. D. Warner, V. Werner, E. Williams, H. L. Liu, and F. R. Xu, Phys. Rev. C **76**, 064302 (2007).

[43] S. Kisyov, D. Bucurescu, J. Jolie, and S. Lalkovski, Phys. Rev. C **93**, 044308 (2016).

[44] D. Bonatsos, Phys. Lett. B **200**, 1 (1988).

[45] P. B. Semmes and I. Ragnarsson, Nuclear Structure Theory Workshop, August 5–16 (1991).

[46] T. Bengtsson and I. Ragnarsson, Nucl. Phys. A **436**, 14 (1985).

[47] E. A. Stefanova, S. Lalkovski, A. Korichi, T. Kutsarova, A. Lopez-Martens, F. R. Xu, H. L. Liu, S. Kisyov, A. Minkova, D. Bazzacco, M. Bergstrom, A. Gorgen, F. Hannachi, B. Herskind, H. Hubel, A. Jansen, T. L. Khoo, Z. Podolyak, and G. Schonwasser, Phys. Rev. C **86**, 044302 (2012).

[48] P. M. Endt, At. Data Nucl. Data Tables **26**, 47 (1981).

[49] N. J. Stone, Table of Nuclear Magnetic Dipole and Electric Quadrupole Moments, Report INDC(NDS)-0658 (2014).